Supporting Information

Control of Nanoplane Orientation in voBN for High Thermal Anisotropy in a Dielectric Thin Film: A New Solution for Thermal Hotspot Mitigation in Electronics

Olivier Cometto,[a,‡] Majid K. Samani,[b,‡] Bo Liu,[c,‡] Shuangxi Sun,[b] Siu Hon Tsang,[d] Johan Liu,[b] Kun Zhou[e] and Edwin H. T. Teo[f,] *

[a] CINTRA CNRS/NTU/THALES, UMI 3288, Research Techno Plaza, 50 Nanyang Drive, Border X Block, Level 6, Singapore 637553. [b] Electronics Materials and Systems Laboratory, Department of Microtechnology and Nanoscience, Chalmers University of Technology, SE-412 96, Sweden. [c] Environmental Process Modelling Centre, Nanyang Environment and Water Research Institute, Nanyang Technological University, 639798, Singapore. [d] Temasek Laboratories@NTU, 50 Nanyang Avenue, Singapore 639798, Singapore. [e] The school of Mechanical & Aerospace Engineering, Nanyang Technological University, 639798, Singapore. [f] School of Electrical and Electronics Engineering, Nanyang Technological University, Block S1, 50 Nanyang Avenue, Singapore 639798. [†] The authors O. Cometto, M. K. Samani and L. Bo contributed equally to this work.

* Corresponding author e-mail: htteo@ntu.edu.sg

Molecular Dynamics simulations

The MD simulation setup was split into the 3 steps below:

1. Preparation of amorphous BN for MD simulation

2. Simulation model for thermal conductivity calculation

3. Simulation model for calculation of interface thermal conductance

Those 3 steps will be explained in more details below.

1. Preparation of amorphous BN for MD simulation

The amorphous BN is generated via a melting and quenching procedure. The procedure starts with a crystalline BN with a diamond lattice structure as the initial configuration. With the periodic boundary conditions applied along all the three directions, the temperature of the crystalline BN is gradually increased from 0 K to 5000 K using a temperature increment step of 1000 K, in a series of molecular dynamics simulations in the NVT ensemble. In each increment step, a heating rate of 100 K/ps is used. After each increment step, the system is thermally equilibrated for 20 ps with the temperature held. Upon the realization of the equilibration at the temperature of 5000 K, the system is cooled down to 300 K at a cooling rate of 1000 K/ps. Once reaching the target temperature of 300 K, the system is switched to the NPT ensemble, and the simulation is conducted for 50 ps to relax the system.

2. Simulation model for thermal conductivity calculation

To investigate the thermal conductivity of the synthesized vertically self-ordered nanocrystalline hexagonal boron nitride (h-BN) thin films, the thermal conductivities of multilayered h-BN nanosheets along the intra-plane and inter-plane directions, as well as the thermal conductivity of the amorphous BN are first calculated. The schematics of the simulation models for the thermal conductivity calculations are shown in Figure S1. The bond length of the

h-BN crystal is set as 1.45 Å,[1] and the interlayer distance between adjacent h-BN layers is set as 3.35 Å.[2] The system length L, width W and thickness H are all set as ~50 Å to represent a crystal size of 5 nm.
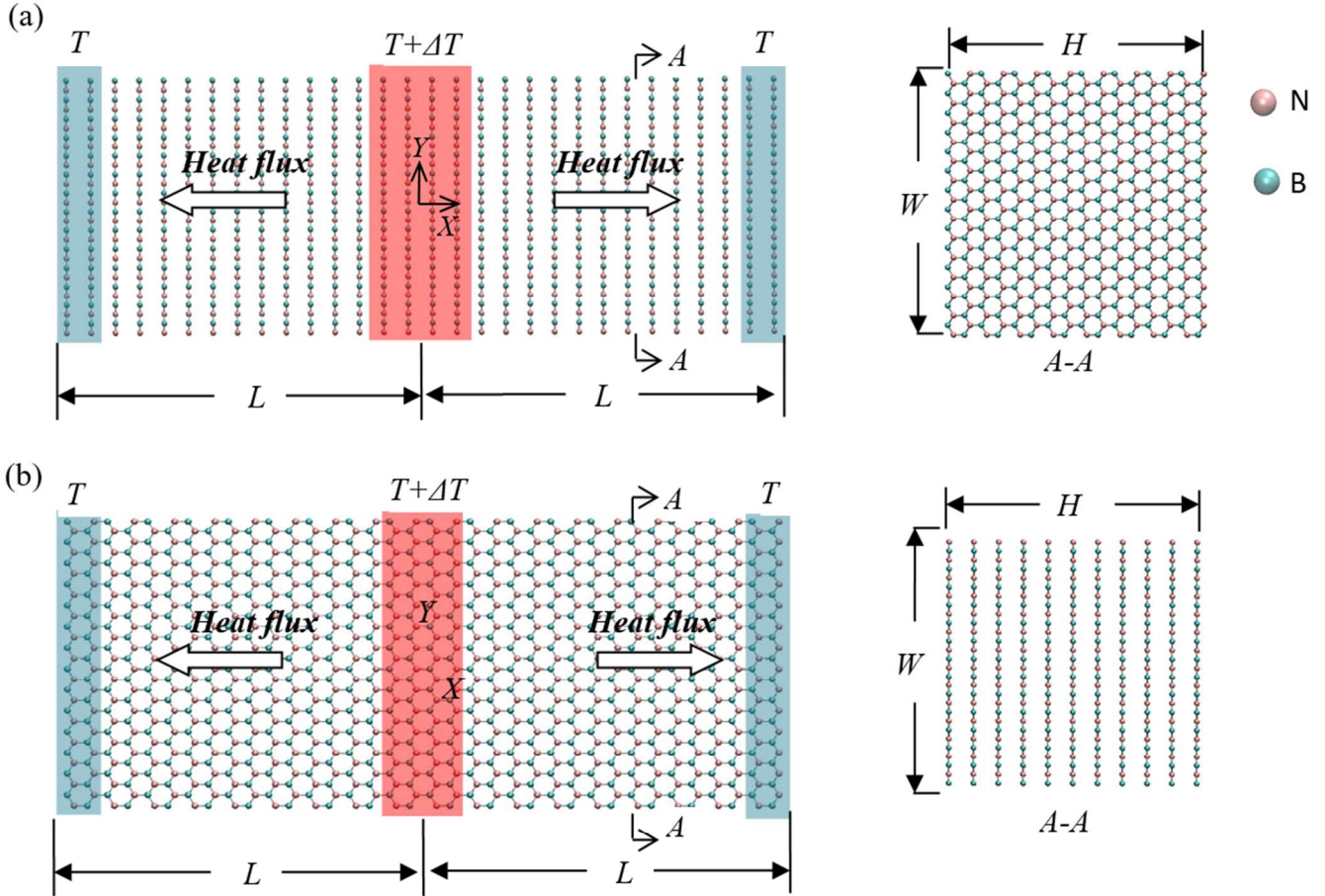

Figure S1. Schematics of the simulation models for the thermal conductivity along (a) the inter-plane and (b) the intra-plane directions of the crystalline h-BN phase. The simulation model for the thermal conductivity of the amorphous BN is similar to that for the crystalline h-BN layers and thus is not shown here. The region highlighted with red in the middle is set as the heat source region and held at the temperature at T+ΔT, and the regions highlighted with blue at the two ends are set as heat sinks and held at a lower temperature of T.

The periodic boundary condition is applied along the longitude x-direction while the free boundary conditions are applied along the y and z-directions. The intra-plane covalent bonding interaction between B and N atoms in the same h-BN layer is described by the Tersoff potential.[3-4] The inter-plane non-covalent bonding interactions for the atoms from different h-BN layers, and that for the atoms between crystalline h-BN and amorphous BN, are modeled by the LJ potential. The corresponding LJ parameters for the B-B and N-N atomic pairs are adopted from the UFF force field[5] and the Lorentz-Berthelot mixing rules are applied to obtain the LJ parameters for the B-N atomic pair. The reverse non-equilibrium molecular dynamics simulation is applied to calculate the thermal conductivity based on the Fourier's law of thermal conduction $J = -\lambda \nabla T$ where J is the heat flux, λ is the thermal conductivity and ∇T is the temperature gradient along the heat flux direction. At first, the initial configuration is well relaxed near $T = 300$ K, which is realized by using the constant pressure and temperature (NPT) ensemble to simulate for 20 ps with the time step $\Delta t = 0.1$ fs. Upon the relaxation of the system, the constant volume and constant temperature (NVT) simulation is conducted for 20 ps to ensure that the system is in an equilibrium state. Afterwards, the system is switched to the constant volume and energy (NVE) ensemble to keep the energy conserved. To create a temperature gradient along the x-direction, the temperature of atoms in the middle region with a width of 2δ as highlighted by red is increased by $\Delta T = 100$ K to serve as a heat source by coupling this region with a Nose-Hoover thermostat. Meanwhile, the atoms in the regions with a width of δ as highlighted with blue at the two ends are kept at $T = 300$ K to serve as heat sinks by coupling them with another two Nose-Hoover thermostats. In Figure S1a and Figure S1b, δ is set as 6.7 Å (width of two h-BN layers) and 4.35 Å (width of two zigzag chains), respectively. Under the NVE ensemble, the simulation is conducted for 100 ps to allow the system to reach a steady state after which a stable

temperature gradient ∇T can be established along the longitude x-direction. Upon the realization

of the stable temperature gradient, the simulation is conducted for another 50 ps to obtain the

heat flux and the time-averaged temperature gradient profile. To calculate the heat flux, the

accumulative energy changes with the simulation time in both the heat source and sink regions

are recorded. The energy changing rate gives the heat flux. To get the gradient profile along the

inter-plane direction (Figure. 1a), the temperature of each h-BN layer is calculated based on the

kinetic energy of all the atoms within the layer. To obtain the gradient profile along the intra-

plane direction (Fig.1b), the entire system is divided into many thin slabs along the x-direction.

The width of each slab is set as 2.175 Å (the width of a zigzag chain). The temperature of each

slab is then calculated based on the kinetic energy of all the atoms within the slab.

3. Simulation model for calculation of interface thermal conductance

For a hybrid system consisting of interfaces, a temperature drop ΔT_{In} at the interface is usually

developed when a heat flux J is imposed into the system, which gives a measurement of the

interface thermal conductance or the Kapitza conductance as $G = J / \Delta T_{\text{In}}$. Figure S2 shows the

simulation model for the calculation. The system size is set as the same as in Figure 1. The

region highlighted with red at the left end with a width of δ is set as the heat source and held at

the temperature of T+ΔT, and the region highlighted with blue at the right end is set as the heat

sink and held at a lower temperature of T. In Figure S2a and Figure S2b, δ is set as 6.7 and 4.35

Å, respectively. Atoms in the thin slabs with a width of ~2 Å near the heat source and sink are

fixed as rigid. The simulation procedure, parameters, and the calculation method of the heat flux

and temperature gradient profile are same to those for the calculation of the bulk thermal

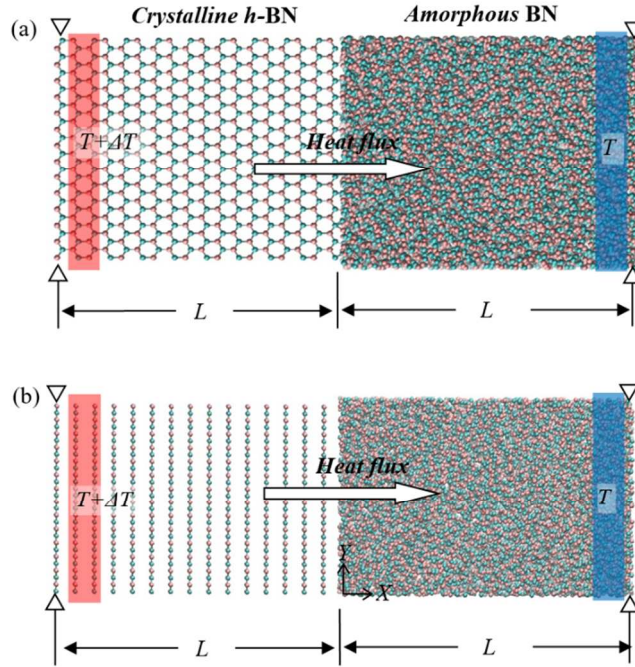conductivity as described above, and thus are not repeated here.

Figure S2. Schematics of the simulation models for the calculation of thermal conductance of the interface between the crystalline h-BN layers and amorphous BN with (a) intra-plane covalent bonding and (b) inter-plane non-covalent bonding. The region highlighted with red at the left end is set as the heat source region and held at the temperature of $T+\Delta T$, and the region highlighted with blue at the right end is set as heat sink and held at a lower temperature of T. Atoms in thin slabs with a width of ~2 Å near the heat source and sink are fixed as rigid.

The phonon spectra for both amorphous and crystalline structure were computed as it is directly linked to the thermal resistance at the interface of a hybrid system. The bigger the mismatch of the phonon spectra of the materials at both sides of the interface,[6-7] the higher the thermal interface resistance. Figure S3 shows that both spectra are not well matched, meaning that there will be a lot of phonon scattering at the interface between both materials, leading to an increased thermal resistance.
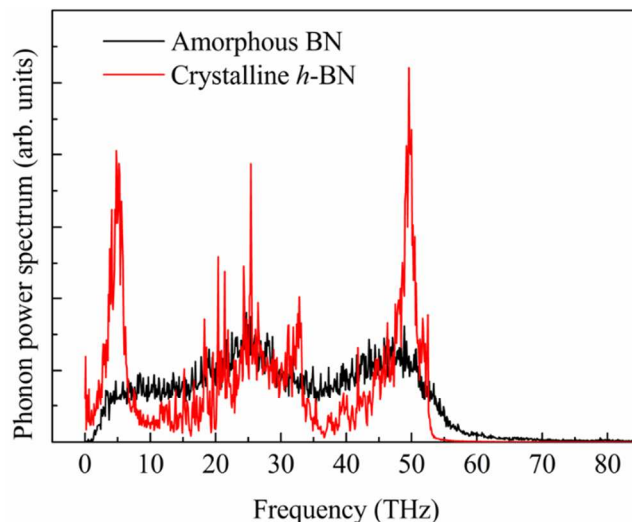
Figure S3. Phonon spectra of the amorphous BN and crystalline h-BN.

FTIR peak ratio computation

This section is meant to explain in detail how the FTIR peak ratio has been computed in this study, which is inspired from previous works.[8-9] First of all, the FTIR raw data was taken from 400 cm^{-1} to 4000 cm^{-1} as seen in Figure S4a. However, since the peaks are located respectively at 780 cm^{-1} and 1380 cm^{-1}, the raw data was truncated between 600 cm^{-1} and 2000 cm^{-1} and smoothed, as sometimes the area of the spectrum at around 2000 cm^{-1} gets slightly noisy and could impact the baseline calculation (Figure S4b). After that, the baseline was computed from both extremes of the truncated spectrum using only two points as shown in Figure S4c. That method was the most easily reproducible between the different FTIR spectra without too much uncertainties. Finally, Figure S4d shows the final results as the baseline got removed from the raw data.
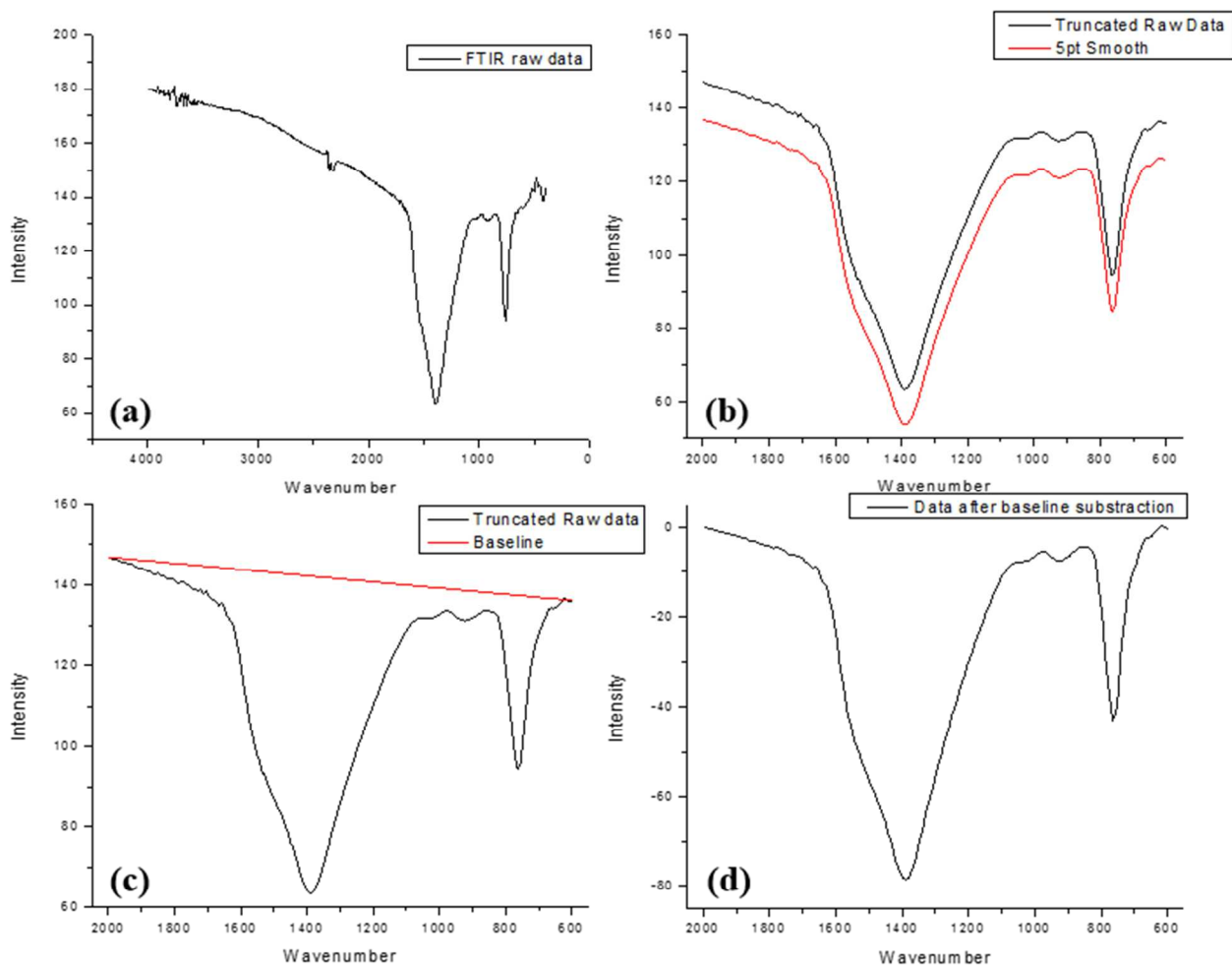
Figure S4. Step by step FTIR data processing before computing the peak ratio. Inset (a) displays the raw data taken from the FTIR measurement. Inset (b) shows the truncated data between 600 and 2000 cm-1 and the curve smoothing. Inset (c) represents the baseline computation and inset (d) is the final result after the baseline has been substracted from the smoothed data.

Once the FTIR data has been processed as shown in Figure S4, the peak ratio can be computed as per Figure S5. In order to facilitate the peak ratio computation, the spectrum gets normalized first in order to have the 0 value as the main in-plane h-BN peak. The ratio $R_{770/1380}$ is then:
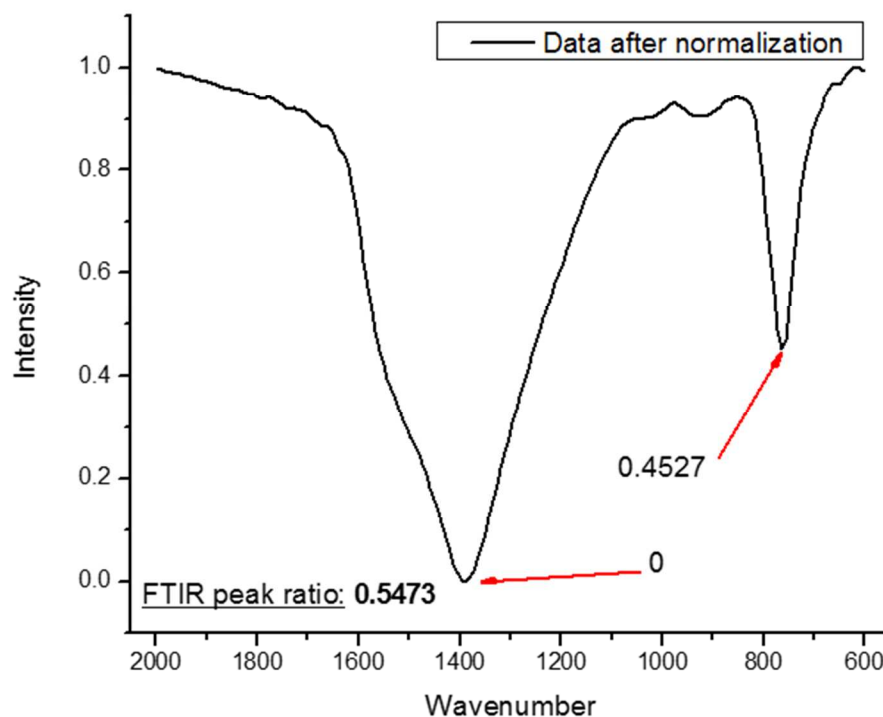
$$R_{770/1380} = 1 - I_{770}$$

Figure S5. Peak ratio computation of a FTIR spectrum for an ordered h-BN thin film. In order to facilitate the ratio computation, the spectrum is normalized between 0 and 1, making the 1380 cm^{-1} peak the 0 value. The ratio would then be 1-I_{770} where I_{770} is the 770 cm^{-1} peak intensity.

This method to compute the peak ratio is accurate to only around 2% mainly due to the baseline computation, which affects the peak's height depending on where the two points for the baseline are taken.

Hot spot crosstalk simulation with COMSOL

Assumptions on the simulation model

The COMSOL Simulation used the following assumptions in order to create the model:

- For the purpose of demonstrating the potential of voBN, we assumed it is possible to get a 100 μm thick voBN film. A thinner layer would not change the physics involved but would make a change in heat spread which is less obvious to see. In addition, the goal

here is to demonstrate the latent capability of voBN as a substrate for heat generating devices.

- We assumed an infinite array of unit cells made of cubes of 100 μm side length with a hot spot located at the bottom (see Figure S6). In addition, as all cells next to each other are identical, there will be no heat gradient between each cell, thus allowing each cell to be considered as an adiabatic system where no heat is lost through the sides of the cube. The faces were then set as thermally insulative, except for the top face where a boundary condition was chosen as fixed 20 degC. This would allow the heat to escape from the top (the same way it would in an actual device), and would allow the model to converge.

- We are only interested in the stationary solution for the system, and all transient studies were avoided.
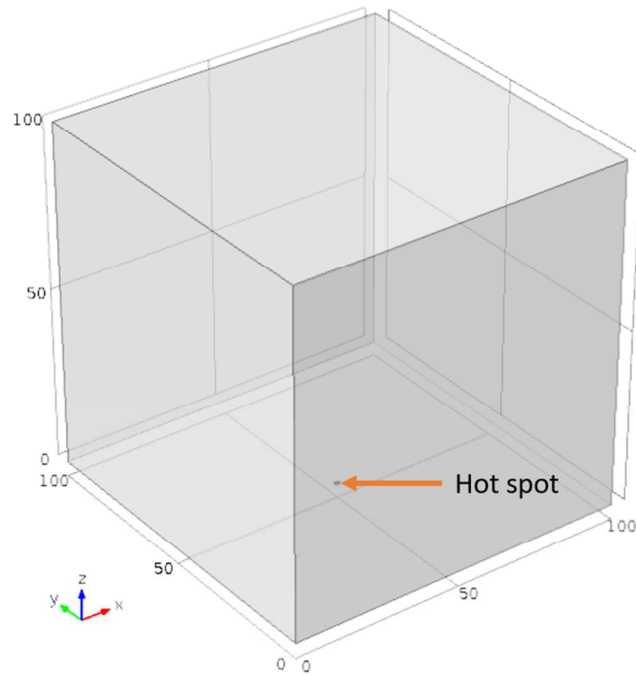

Figure S6. Unit cell where thermal crosstalk will be simulated.

Set of equations used to solve the model

The standard set of equations used by the COMSOL Heat Transfer Module were used:

- Heat transfer equation across the volume (Fourier's Law): $\nabla T + \nabla . \vec{q} = Q$ where $\vec{q} = -k \nabla T$. $\vec{q}$ is the heat flux vector and Q is the heat source and/or sink.

- To represent the adiabatic system, the sides were set to behave accordingly to the following equation: $-\vec{n}.\vec{q} = 0$ meaning that there is no temperature gradient across the boundary.

- The top face of the cube has the boundary condition of being set to 20 degC and would play the role of a heat sink: $T = 20$ degC at the boundary.

- For the hot spot, a 1 μm x 1 μm zone at the bottom would generate a 0.1 mW heating power evenly across the surface: $-\vec{n}.\vec{q} = Q_{heat}$ where $Q_{heat} = 10^8$ W.m^{-2} (0.1 mW over 1 μm2). The hot spot is represented by a square surface instead of a point as the former would introduce singularities, i.e. the model would have to simulate a finite amount of energy flowing through an infinitely small space, which is equivalent to $Q_{heat} = +\infty$.

Mesh design

The mesh is an essential part of simulation design and an insufficient mesh precision in zones with high temperature changes would drastically change the results. For instance, Figure S7 shows how a bad mesh (Figure S7a) would impact the results, compared to a good one (Figure S7b). It can be noted that a bad mesh as seen in Figure S7c contains only two elements for the hot spot, while the good mesh contains more than 20 elements (Figure S7d), with the surrounding mesh around the hot spot being quite detailed as well, in order to properly compute the large gradients of temperature around that area. The mesh used in the simulation inside the whole cell was a tetrahedral mesh with a minimum element size of 1.4 μm and a maximum size of 10 μm. Around and inside the hot spot, the mesh was refined with a minimum element size

going as low as 0.02 μm and a maximum size of 2 μm. Increasing the mesh quality further did not improve the results further, and exponentially increased the computing time.
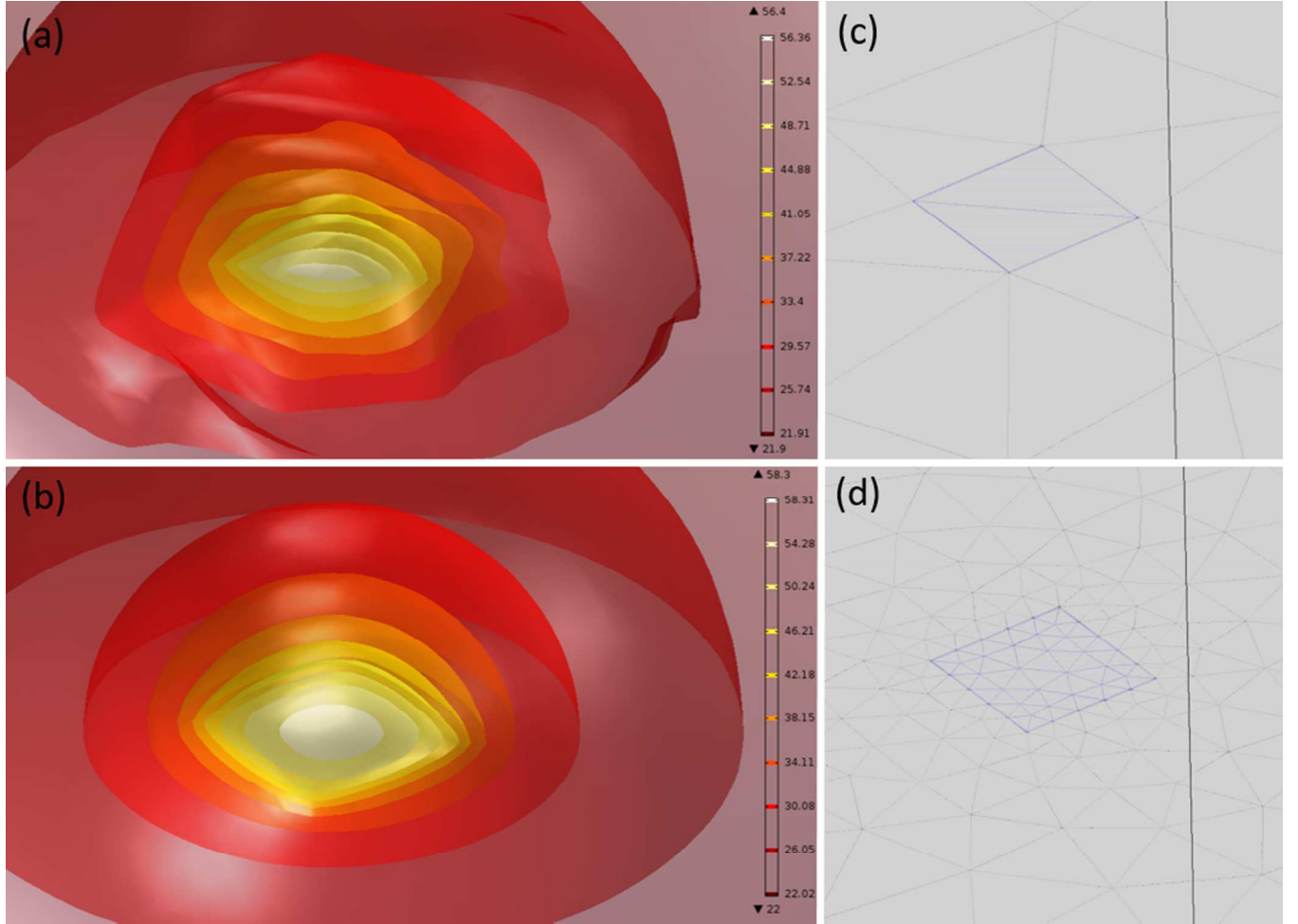

Figure S7. Comparison of isothermal contours simulations with SiO_2 around the hot spot with a bad mesh (a) and a good mesh (b). It can also be observed that the computed temperatures between both simulations are not the same. Inset (c) and (d) show the difference in meshing quality for both simulations.

Directional heat extraction

The thermal conductivity anisotropy property of voBN is shown in the COMSOL simulations by the shape of the isothermal contours as shown in Figure S8. Indeed, the increased TC in the z direction has the consequence of stretching the isothermal contours in the vertical direction,

which indicates an increased vertical heat extraction. In comparison, SiO_2 induces spherically shaped isothermal contours due to its isotropic thermal conductivity.
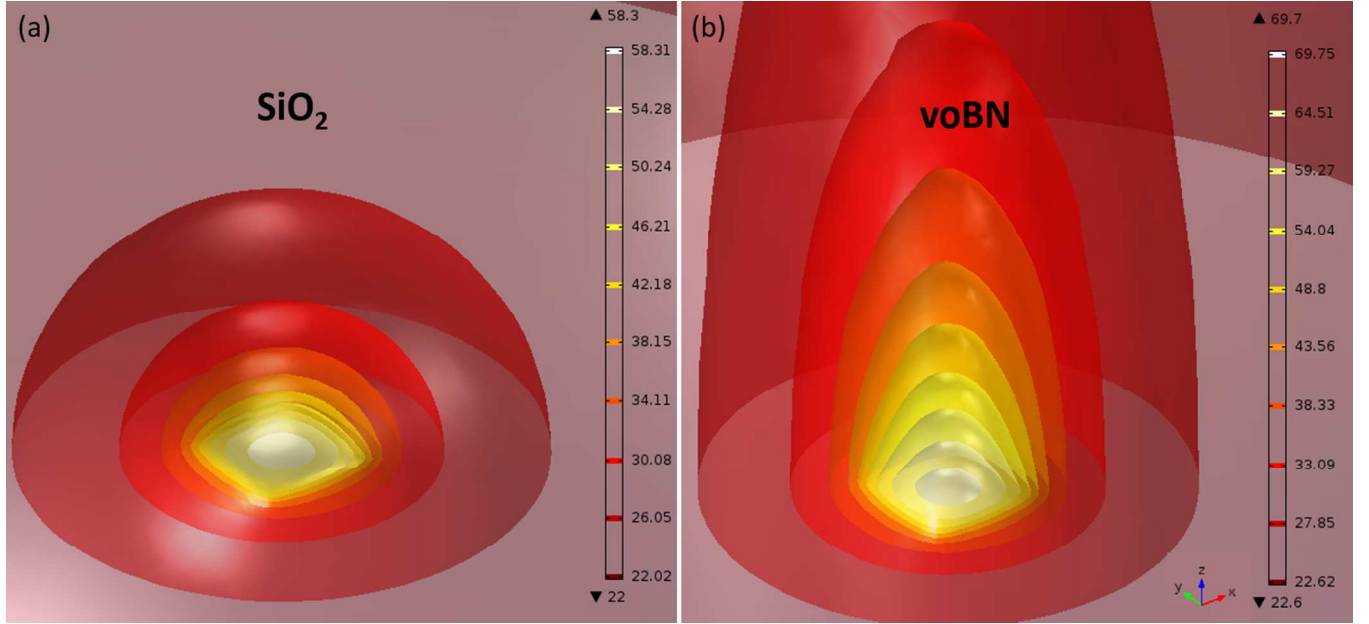

Figure S8. Isothermal contours around the hot spot for SiO_2 (a) and voBN (b). The spherical contour shape in SiO_2 is the typical response from isotropic materials while the stretched contours along the z axis for voBN is characteristic of a material with greater thermal conductivity along the z axis compared to the x and y axis.

Dielectric constant computation

A rough approximate of the dielectric constant was computed in this work. A capacitor was made with voBN as the dielectric material and by measuring its complex impedance, the dielectric constant was extracted. This technique relies on using the measured capacitance C to extract the dielectric constant ε_r via the formula from a parallel plate capacitor:

$$C = \varepsilon_r \varepsilon_0 \frac{A}{t}$$

ε_0 is the permittivity of free space and equals approximately 8.854×10^{-12} F.m^{-1}. A is the capacitor plate area, and t is the dielectric thickness. This formula is valid only in the condition

where t is very small next to the smallest chord of the capacitor plate. Figure S9 shows the capacitor design used to compute C.
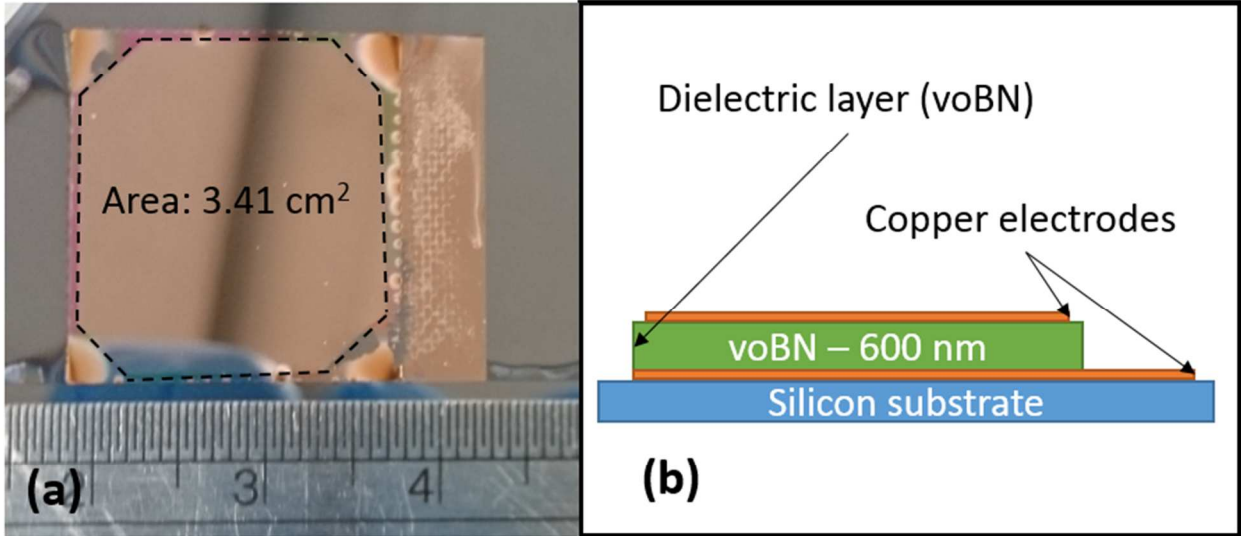

Figure S9. Inset (a) is a photo of the device, with the area of the top copper electrode computed to be 3.41 cm². Inset (b) is a schematic of the design in cut view. The voBN film thickness was computed to be 600 nm via surface profiling.

Using a probe station to sweep the device across frequencies ranging from 1 kHz up to 1 MHz, the complex impedance of the device was retrieved (assuming the device behaves like a RC series circuit). From the definition of the complex impedance Z, we get the following equalities:

$$\begin{cases} Z = R + jX \\ Z = R + \dfrac{1}{j\omega C} \end{cases} \leftrightarrow X = \frac{-1}{\omega C} \leftrightarrow Cf = \frac{-1}{2\pi X}$$

R and X are the real and imaginary parts of the impedance, ω is the pulsation and $\omega = 2\pi f$ where f is the frequency of the sweep. The data retrieved is plotted in Figure S10:
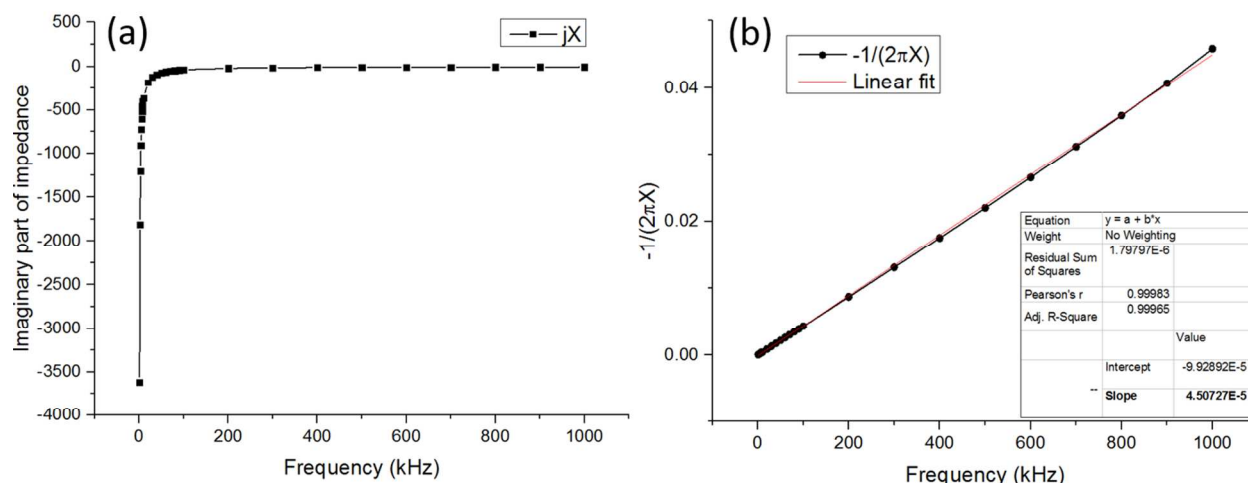
Figure S10. Inset (a) is a plot of the imaginary part of the complex impedance. Inset (b) plots $\frac{-1}{2\pi X}$ and is linearly fitted in order to extract the capacitance. The computed slope is 45×10^{-6}, which gives a capacitance of 45 nF (there is a factor 1000 due to the plot axis being in kHz instead of Hz).

Once the capacitance of 45 nF was acquired, the dielectric constant of voBN was finally computed to be approximately 8.94, which is higher than what is reported in the literature,[10] and could be due to either inaccuracies in the measurement method, and/or the presence of lanthanum in the thin film due to the growth conditions. Either way, the main objective here is to show that voBN remains a dielectric and can be used to passivate electronic devices.

References

1.   Warner, J. H.; Rummeli, M. H.; Bachmatiuk, A.; Buchner, B., Atomic Resolution Imaging and Topography of Boron Nitride Sheets Produced by Chemical Exfoliation. *ACS Nano* **2010,** *4* (3), 1299-304.
2.   Zeng, H.; Zhi, C.; Zhang, Z.; Wei, X.; Wang, X.; Guo, W.; Bando, Y.; Golberg, D., "White graphenes": Boron Nitride Nanoribbons via Boron Nitride Nanotube Unwrapping. *Nano Lett.* **2010,** *10* (12), 5049-55.
3.   Tersoff, J., Modeling Solid-State Chemistry: Interatomic Potentials for Multicomponent Systems. *Physical Review B* **1989,** *39* (8), 5566-5568.
4.   Matsunaga, K.; Fisher, C.; Matsubara, H., Tersoff Potential Parameters for Simulating Cubic Boron Carbonitrides. *Japanese Journal of Applied Physics* **2000,** *39* (Part 2, No. 1A/B), L48-L51.
5.   Rappe, A. K.; Casewit, C. J.; Colwell, K. S.; Goddard, W. A.; Skiff, W. M., UFF, a Full Periodic Table Force Field for Molecular Mechanics and Molecular Dynamics Simulations. *J. Am. Chem. Soc.* **1992,** *114* (25), 10024-10035.

6.   Liu, B.; Meng, F.; Reddy, C. D.; Baimova, J. A.; Srikanth, N.; Dmitriev, S. V.; Zhou, K., Thermal Transport in a Graphene–MoS2 Bilayer Heterostructure: a Molecular Dynamics Study. *RSC Adv.* **2015,** *5* (37), 29193-29200.

7.   Liu, B.; Reddy, C. D.; Jiang, J.; Baimova, J. A.; Dmitriev, S. V.; Nazarov, A. A.; Zhou, K., Morphology and in-Plane Thermal Conductivity of Hybrid Graphene Sheets. *Appl. Phys. Lett.* **2012,** *101* (21), 211909.

8.   Dworschak, W.; Jung, K.; Ehrhardt, H., Growth Mechanism of Cubic Boron Nitride in a R.F. Glow Discharge. *Thin Solid Films* **1995,** *254* (1–2), 65-74.

9.   Zhang, X. W.; Boyen, H. G.; Yin, H.; Ziemann, P.; Banhart, F., Microstructure of the Intermediate Turbostatic Boron Nitride Layer. *Diamond Relat. Mater.* **2005,** *14* (9), 1474-1481.

10.   Geick, R.; Perry, C. H.; Rupprecht, G., Normal Modes in Hexagonal Boron Nitride. *Physical Review* **1966,** *146* (2), 543-547.